https://doi.org/10.5194/wes-2022-7
Preprint. Discussion started: 8 February 2022
© Author(s) 2022. CC BY 4.0 License.

eawe european academy of wind energy
Open Access WIND ENERGY SCIENCE DISCUSSIONS

Quantifying the effect of blockage for wind farm layout optimization

Ethan Young[1], Jeffery Allen[1], John Jasa[1], Garrett Barter[1], and Ryan King[1]
[1]National Renewable Energy Laboratory, Boulder, CO
Correspondence: Ethan Young (ethan.young@nrel.gov)

Abstract. Wind plant blockage is a phenomenon where the presence of a large wind farm creates a disturbance to air flow external to the farm itself that is not accounted for by wake effects. This is typically manifested as a slowdown in wind velocity upstream from a plant, which can be shown to decrease power production. Knowing a priori how a wind farm's layout will generate blockage could help to improve the accuracy of AEP calculations and suggest more blockage-optimal turbine layouts. In this study, we consider the effect of wind plant blockage and perform multiple types of layout optimization to reduce blockage while solving the flow physics using computational fluid dynamics. We present a variety of methods to quantify this blockage effect, ranging from localized measurements taken in the proximity of each turbine to farm-wide integral measurements designed to capture the velocity decrease in a more global way. We then investigate each blockage metric using simple case studies designed to isolate effects due to layout changes. While all metrics show sensitivity during this testing, the integral metrics better avoid spurious effects due to waking and are better suited to evaluating blockage which we find to be a cumulative effect. We then perform multiple farm layout optimizations using these blockage metrics as objectives and find that in the absence of a power production constraint the optimized layouts tend to minimize disturbance to the surrounding flow by creating streamwise rows of turbines. Finally, we present a power-constrained layout optimization which explicitly illustrates the trade-off between designing for blockage and power. This work presents a variety of different blockage definitions and offers a set of recommendations regarding their deployment, expected behavior, and viability for consideration as part of layout planning.

1 Introduction

Modeling and simulation tools to optimize wind farm layout are typically structured with the goal of maximizing the total power output of the farm (Allen et al., 2020). This is seen in both optimizations relying on mid-fidelity computational fluid dynamics (CFD) simulations as well as those relying on wake superposition techniques for real-time operation (NREL, 2021a). However, recent work has shown the value of considering alternative objectives, including maximizing the ability of a turbine to steer its wake during yawed operation or the ability of a turbine to entrain additional momentum from overhead (Allen et al., In Final Review). The importance of blockage, most often defined as the slowdown of streamwise velocity in the region upstream from a turbine or farm, has received increased attention for reasons ranging from the impact on wildlife (Quon et al., 2021) to the discrepancy between predicted and observed power in newly-constructed plants (Bleeg et al., 2018). Previous work has examined engineering models to capture the effects of blockage (Branlard et al., 2020). Formalizing a method to

https://doi.org/10.5194/wes-2022-7
Preprint. Discussion started: 8 February 2022
© Author(s) 2022. CC BY 4.0 License.

eawe european academy of wind energy
Open Access WIND ENERGY SCIENCE DISCUSSIONS

measure this blockage effect in a manner that facilitates layout optimization enables turbine array designs that balance total power output while also mitigating the impact on upstream conditions.

In the current work, we present a variety of blockage definitions and evaluate their suitability as optimization objectives. We determine suitability through a suite of tests designed to isolate and measure the response when modifying various features of farm layout. To adequately characterize blockage, we expect the metrics to: (i) demonstrate sensitivity with respect to modifying layout features, (ii) have a more pronounced effect when the layout more closely resembles a solid obstacle due to turbine density and/or arrangement, and (iii) be relatively easy to compute and stable with respect to small perturbations. We use the results from this testing along with these criteria to tune each blockage metric to best capture the effect on the simulated velocity before solving a series of layout optimization problems. Analyzing these blockage-optimized layouts reveals patterns in the turbine placement that typify a minimal disturbance to the surrounding flow. Recognizing that a pure blockage optimization might considerably diminish the total power output of the farm, we also present a power-constrained blockage optimization which enforces a minimum level of power output while still minimizing blockage. The paper is organized with the goal of first providing a background on measuring blockage and its effects, Sections 2 and 3, respectively, next demonstrating the potential value of a blockage-aware layout optimization, Section 4, and finally discussing the current findings and overall relevance of blockage as an optimization objective in Section 5.

2 Methodology

We perform these studies using `WindSE`, a software package for the simulation and optimization of wind farms NREL (2021b). `WindSE` relies heavily on two Python packages, `FEniCS` and `dolfin-adjoint`, which have considerable crossover but are generally responsible for assembling and computing the solution of differential equations using the finite-element method and coordinating the calculation of the discrete adjoint for optimization purposes Logg et al. (2012); Funke and Farrell (2013).

2.1 Fluid Solver

The fluid is simulated using the steady-state, incompressible Navier-Stokes equations:

$$\rho(\mathbf{u}\cdot\nabla\mathbf{u}) = -\nabla P + \nu\nabla^2\mathbf{u} + \mathbf{F} \tag{1}$$

$$\nabla\cdot\mathbf{u} = 0, \tag{2}$$

where $\mathbf{u}$ is the fluid velocity, P is the pressure, $\mathbf{F}$ is the thrust force arising from the turbines, and ρ is the fluid density. The total viscosity, ν, is the sum of a background viscosity and a spatially-varying eddy viscosity governed by a characteristic mixing length, ℓ_{max}. The velocity and pressure fields are discretized in space using first-order, tetrahedral finite elements. The turbine forces are represented as non-rotating actuator disks which smoothly project the blade forces over the rotor-swept area:

$$\mathbf{F}(x,y,z) = \frac{1}{2}\rho A C_t' \mathbf{u}^2 T(x) R(y,z), \tag{3}$$

https://doi.org/10.5194/wes-2022-7
Preprint. Discussion started: 8 February 2022
© Author(s) 2022. CC BY 4.0 License.

eawe european academy of wind energy
Open Access WIND ENERGY SCIENCE DISCUSSIONS

where A is the rotor-swept area, a function of rotor diameter, D, C_t' is a modified thrust coefficient defined as $C_t/(1-a)^2$ using a constant axial induction factor, a, T is a linear Gaussian field capturing the streamwise dimension of the rotor, and R is a cylindrical Gaussian field capturing the spanwise dimension.

2.2 Adjoint Calculation and Optimization Solver

With the velocity and pressure field solved for, we turn our attention to the optimization framework that will modify the layout via the definition of turbine forces to achieve a given blockage objective. We use `dolfin-adjoint` within `FEniCS` to efficiently compute accurate gradients for the wind farm design problem and this process is described in previous work Allen et al. (2020). Gradient-based optimizers are more computationally effective at solving continuous large-scale optimization problems than gradient-free methods as detailed by Lyu et al. (2014). This choice allows us to use `SNOPT`, developed by Gill et al. (2002), a sparse nonlinear sequential quadratic programming method that effectively solves local optimization problems using relatively few function and gradient evaluations.

`SNOPT` uses a continuous augmented Lagrangian merit function and the Hessian of the Lagrangian is approximated using a limited-memory quasi-Newton method Gill et al. (2002). It solves large-scale problems with many nonlinear constraints and a continuous objective, but cannot optimize discrete problems. We use `SNOPT` to solve every optimization case presented in this paper. To access `SNOPT`, we use `pyOptSparse` Wu et al. (2020), an open-source framework that provides a common API to multiple different optimizers.

2.3 Blockage Metric Definition

In order to perform a meaningful optimization study, it is first necessary to formalize a metric to measure blockage. Although there does not seem to be a formal mathematical definition of blockage, the general consensus is that blockage is a disturbance of the flow surrounding a wind farm that is caused by that farm's presence. The most commonly discussed form of this disturbance is a slowdown of wind upstream of the farm, usually expressed as a percentage reduction of the freestream or with units of velocity deficit Bleeg et al. (2018); Nygaard et al. (2020); McTavish et al. (2015). In this case, a simple exercise to quantify the effect would be to evaluate the velocity field with and without turbines and compute the difference. Although other measurements can be devised to capture blockage effects, for example, wake expansion of tip-vortex cores as they are advected downstream McTavish et al. (2014), measurements involving velocity are much more naturally implemented in WindSE's pressure-velocity RANS solver with existing information versus a calculation relying on secondary and/or derived quantities.

Having decided that disturbance of the velocity field is the most natural definition of blockage, attention turns to the details of its implementation. Three approaches were identified, depicted in Figures **??**-**??**, with the principal difference being where the fluid velocity is measured. In the first metric, the velocity of the fluid is measured at a single point upstream or overhead relative to a single turbine or the farm. This metric was chosen as it is the simplest type of measurement and mimics data available from real world meteorological (MET) towers. To facilitate the distributed calculation of adjoints, the point measurement is

https://doi.org/10.5194/wes-2022-7
Preprint. Discussion started: 8 February 2022
© Author(s) 2022. CC BY 4.0 License.

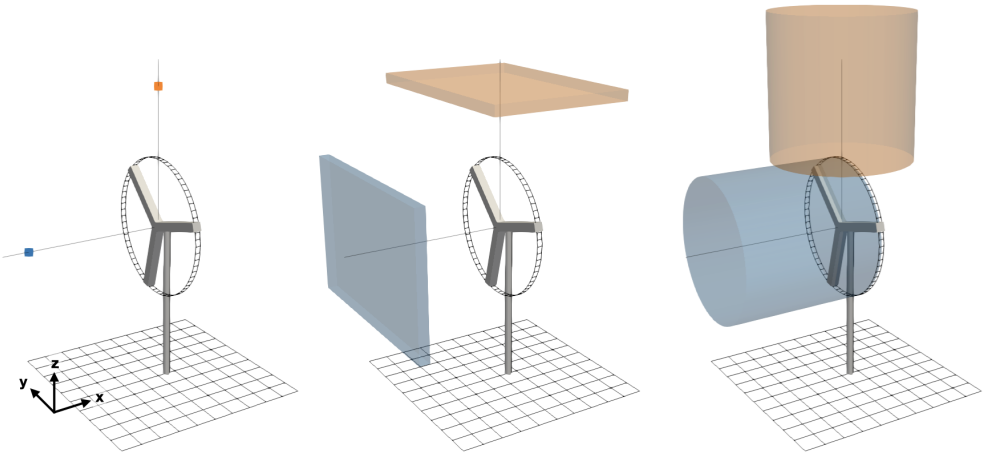

Figure 1. The three different metrics and associated measurement regions for capturing the effect of blockage, blue/orange indicates the upstream/overhead orientation, rotor blades and turbine towers are included here for illustrative purposes only.

actually represented as a small Gaussian sphere. The expression for this metric is:

$$J = \frac{1}{V} \iiint u \exp\left(-\left(\frac{(x-x_0)^2 + (y-y_0)^2 + (z-z_0)^2)}{r_p} \right)^6 \right) dV, \tag{4}$$

where (x_0, y_0, z_0) is the evaluation location, r_p is the radius of the Gaussian sphere, V is the volume, and u is the streamwise velocity.

The second blockage metric extends the measurement area from a single point to a thin yz- or xy-box oriented either upstream or overhead of the farm respectively. Since this thin box extends over some finite volume, the final blockage metric is calculated by integrating the streamwise velocity component inside the box and then normalizing by the box's volume. The dimensions of the box can be restricted to cover a single, leading-row turbine or extended to cover the projected area of the farm in the $x-$ or $z-$direction. With its farm-wide coverage, this metric represents a more global view of blockage vs the local view provided by the point. The expression for this metric is:

$$J = \frac{1}{V} \int_{x_0}^{x_1} \int_{y_0}^{y_1} \int_{z_0}^{z_1} u \, dxdydz, \tag{5}$$

where, (x_0, y_0, z_0) and (x_1, y_1, z_1) are the two opposite corners of the box. The final blockage metric follows the volumetric approach of the thin plate but in a more regionalized fashion; cylindrical volumes defined by the intersection of radial and streamwise Gaussian fields are constructed upstream or overhead relative to each turbine in the farm. These cylinders are very similar in construction to the actuator disk's Gaussian kernel and were chosen to mimic a power optimization. The fact that these cylinders are local to each turbine results in this metric being a mix of both local and global perspectives on blockage.

https://doi.org/10.5194/wes-2022-7
Preprint. Discussion started: 8 February 2022
© Author(s) 2022. CC BY 4.0 License.

eawe european academy of wind energy
Open Access WIND ENERGY SCIENCE DISCUSSIONS

The expression for upstream cylinders is:

$$J = \sum_{i}^{N} \left[\frac{1}{V} \iiint u \exp\left(-\left(\frac{x - x_i - L/2}{L} \right)^6 - \left(\frac{(y-y_i)^2 + (z-z_i)^2}{r_c} \right)^6 \right) dV \right], \tag{6}$$

or for overhead cylinders

$$J = \sum_{i}^{N} \left[\frac{1}{V} \iiint u \exp\left(-\left(\frac{z - z_i - D - L/2}{L} \right)^6 - \left(\frac{(x-x_i)^2 + (y-y_i)^2}{r_c} \right)^6 \right) dV \right],$$

where, (x_i, y_i, z_i) is the hub height location of the ith turbine, L is the length/height of the cylinder, r_c is the cylinder radius, and D is the rotor diameter.

In all cases, each metric is first evaluated without turbine forces to establish a baseline measurement, J_b. The simulation is then repeated with turbines, J_t, and the blockage measurement is calculated as $J = J_t - J_b$. Thus, blockage < 0 m/s indicates a slowdown of the fluid due to the turbines while blockage > 0 m/s indicates a speed up of fluid, where the latter may occur in overhead orientations measuring a redirection of flow up and over the farm.

It is worth noting that both the point and box metrics are implemented in a singular manner that is generally not associated with individual turbines. That is, although they may be positioned based on the average turbine location or projected farm area, they do not capture blockage on a turbine-by-turbine basis. In contrast, the Gaussian cylinders are associated with every turbine in the farm with some measurements occurring within the interior of the farm. This decision exposes the cylinder metric to potential biasing from the wake effects, but may yield potentially important information about regionalized blockage effects.

3 Blockage

Here, we demonstrate the behavior of the different blockage metrics presented in Section 2.3. To characterize their effectiveness, we designed a set of case studies to capture the major components of plant layout. These components include the total number of turbines (Section 3.1), the spacing between turbines (Section 3.2), and the staggering between rows (Section 3.3). These parameter sweeps were designed to study the metrics' responses to isolated layout changes and to determine the suitability of the blockage metrics for a full wind-farm layout optimization. For each test case, all turbine properties are set according to the International Energy Agency (IEA) definition for a 3.4 MW land-based reference turbine Bortolotti et al. (2019). The relevant specification details are shown in Table 1. The complete details of the simulation and domain parameters used for each test case are available at the `WindSE` Github repository[1].

In each of the test cases, the location of the point and box blockage measurements remained the same. The upstream point was fixed at $3D$ upstream from the central leading turbine's hub while the overhead point was $1.5D$ above the hub height of the central leading turbine. The upstream box was centered $3D$ upstream from the leading ledge of the farm with a thickness of D while the overhead box was centered at $1.5D$ above the farm's hub height with a thickness of D. The large area of the box was chosen to extend $\pm D$ past the maximum extent of the farm border in the streamwise, spanwise, and ground-normal directions.

[1] https://github.com/NREL/WindSE/tree/master/demo/undocumented/blockage_metrics

https://doi.org/10.5194/wes-2022-7
Preprint. Discussion started: 8 February 2022
© Author(s) 2022. CC BY 4.0 License.

eawe european academy of wind energy
Open Access WIND ENERGY SCIENCE DISCUSSIONS

Table 1. Parameter values and simulation definitions applied to all studies.

Parameter	Value	Units
Rotor diameter, D	130	m
Hub height, HH	110	m
Axial induction, a	0.33	
Yaw Angle	0	deg
Hub Height Velocity, $\mathbf{u}_{ref}$	8	m/s
Inflow Direction	West	
Kinematic Viscosity, ν_0	1.5×10^{-5}	Pa·s
Density, ρ	1	kg/m^3
Mixing Length, ℓ_{max}	15	m

The cylindrical kernel volumes are defined on a per-turbine basis and the locations relative to each turbine are defined with a consistent set of parameters. Each upstream cylinder has a face defined by the rotor-swept area which extends upstream for $3D$ while each overhead cylinder begins at the edge of the rotor-swept area and extends upward for $3D$ aligned with the turbine's mast.

3.1 Systematic Layout

This case study was designed to reveal blockage effects caused by additional turbines in both the downstream and spanwise directions. The value of each blockage metric was measured for a single turbine, then re-measured with an increasing number of downstream turbines until finally simulating 7 turbines aligned in the streamwise direction. This test was then repeated for increasingly wide farms comprised of 3, 5, and 7 spanwise rows to test the effect of enhanced blockage in the presence of spanwise neighbors. The behavior of each metric is shown as a function of an increasing number of downstream turbines for each of the width-varied farms in Figure 2. It is worth reiterating that the blockage in these case studies is compared with a turbine-free measurement, so positive blockage can be interpreted as an increase in velocity while negative blockage can be interpreted as a decrease in velocity.

The first major trend we see is that the upstream variants experience decreased streamwise velocity while the overhead variants experience increased streamwise velocity. With each of the upstream measurement variants, the slowdown increases with additional streamwise neighbors, though the relationship for spanwise neighbors is less clear. For the overhead variants, the effect of including additional spanwise neighbors is an increase in the streamwise velocity over the top of the farm. The relationship with additional streamwise neighbors is less evident, as the point metric shows decreased blockage but both the box and cylinder show increasing blockage.

There are some specific trends worth noting. First, the upstream point metric is the only metric that does not experience monotonic change in blockage with increasing number of spanwise neighbors. Initially, we thought this might be a mesh-

https://doi.org/10.5194/wes-2022-7
Preprint. Discussion started: 8 February 2022
© Author(s) 2022. CC BY 4.0 License.

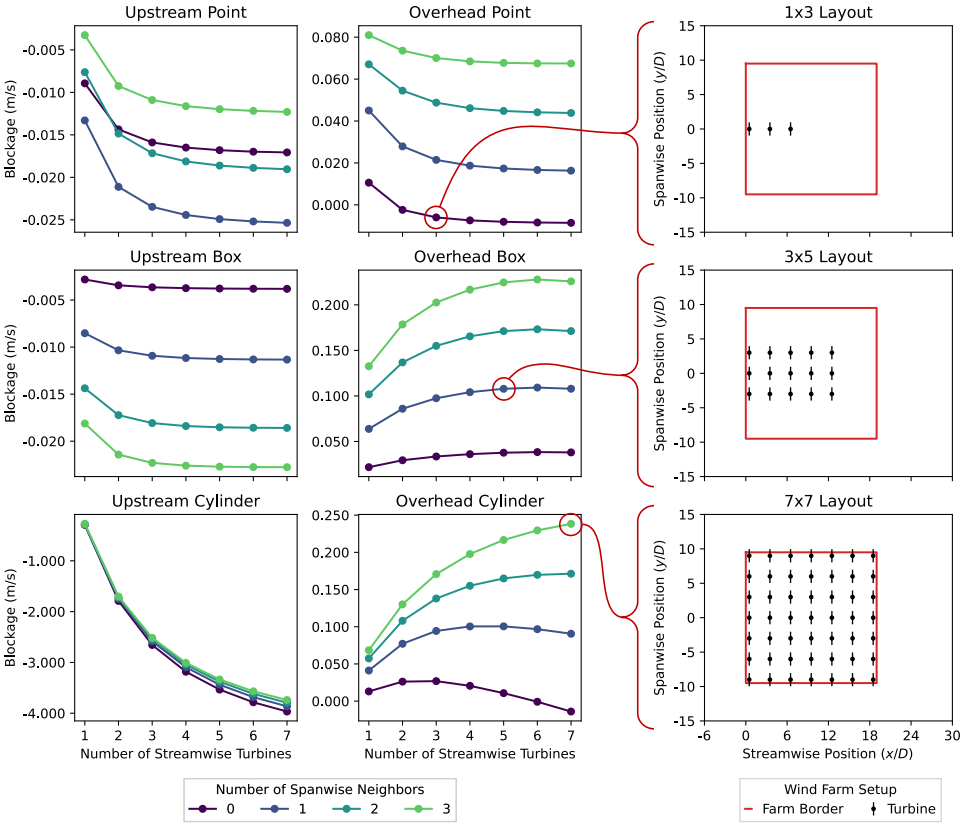

Figure 2. Measured blockage as a function of farm size; Top: the upstream and overhead point measurements, Middle: the upstream and overhead boxes, Bottom: the upstream and overhead cylinders.

related anomaly; however, refining the mesh does not change this behavior. Further research is needed to understand why this trend happens. In Section 5 we discuss why the point metrics might not be the best blockage metrics for optimization. Another observed trend is that the upstream cylinder metric has the largest range of blockage values. This likely stems from this measurement being highly influenced by wake effects due to defining measurement regions directly behind one or more upstream turbines. The box metrics behave in a way that seems indicative of a suitable blockage metric for optimization. For both variants, the blockage effect resulting from adding an additional downstream turbine is enhanced with increasing numbers of spanwise turbines. It is important to note that a full layout optimization would operate with a fixed number of turbines, i.e., not adding or removing turbines to suit a particular definition of blockage. Here, the decision to model varying numbers of turbines was made for computational convenience and to fully isolate any change in blockage due to farm size.

https://doi.org/10.5194/wes-2022-7
Preprint. Discussion started: 8 February 2022
© Author(s) 2022. CC BY 4.0 License.

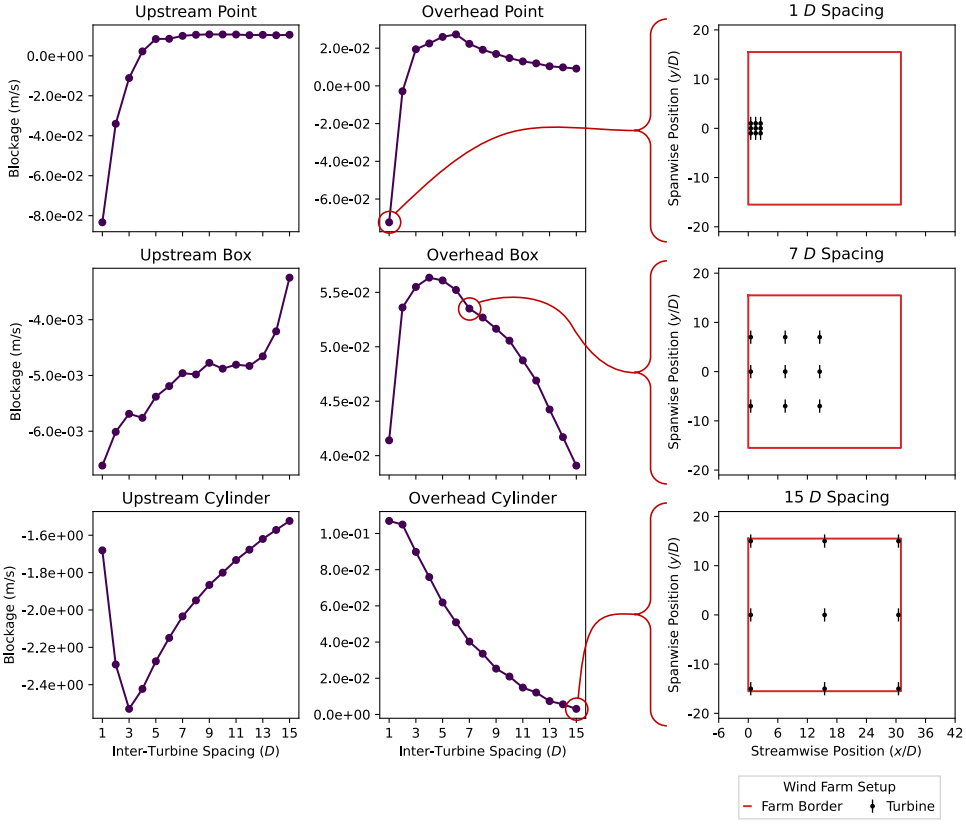

Figure 3. Measured blockage as a function of turbine separation; Top: the upstream and overhead point measurements, Middle: the upstream and overhead boxes, Bottom: the upstream and overhead cylinders.

3.2 Spacing

In contrast to the previous study, this case study focuses on a fixed number of turbines with varied spacing. We vary the the streamwise and spanwise spacing of a 3×3 square grid between $3D$ and $15D$ in increments of $1D$. This is an attempt to isolate the effect of inter-turbine spacing on blockage. The blockage metrics are defined with the locations and sizes presented in Section 3. The results of this spread test are presented as a function of the turbine spacing in Figure 3. As with the systematic farm, the upstream variants produce a negatively-signed blockage indicating a slowdown while the overhead variants reveal blockage effects as a speedup. Measuring the upstream cylinder blockage with a spacing $< 3D$ results in overlapping Gaussian kernels, which further complicates the effect being reported in those cases.

When the spacing is $< 6D$ the farm seems to behave more like a single, solid obstacle, which enhances the blockage effect by redirecting more of the incoming flow. However, past $6D$, the turbines sufficiently separated such that the fluid can easily flow resulting in minimal blockage effects. This is particularly evident in the overhead point and box predicting a maximum

https://doi.org/10.5194/wes-2022-7
Preprint. Discussion started: 8 February 2022
© Author(s) 2022. CC BY 4.0 License.

blockage at roughly $6D$. This could explain why most of the metrics tend to stabilize or trend to zero as the spacing increases. A notable exception is the upstream box where the blockage effect starts to accelerate around $13D$. Since the domain of integration for the upstream box only extends $1D$ beyond the farm in the spanwise direction, it is possible that the domain of integration is no longer large enough to fully capture the blockage effects and, thus, some is lost.

3.3 Skewness

Finally, we study the effect that farm skewness has on the blockage metrics. We know that the performance of a gridded wind farm aligned with the dominant wind direction will suffer greatly from wake losses; however, the effect that modifying the alignment of such a farm has on blockage remains to be seen. In this test, we examine progressively skewed wind farms, where the original grid is modified so that each subsequent column is shifted laterally relative to the column in front of it. We begin with a square 5x5 gridded wind farm with a consistent streamwise and spanwise spacing of $3D$. From here, we skew the farm by laterally shifting each subsequent column of the farm by a certain amount. As we skew the wind farm, we see differing trends for each of the blockage metrics as shown in Fig. 4. Unlike the previous two studies, the trends for how skewness affects blockage are a bit more difficult to interpret. There seem to be two primary modes corresponding to when turbines are aligned in the streamwise direction and when downstream turbines are perfectly spaced in the windows formed by upstream turbines. The first mode occurs when there is zero skew and again when there is $3D$ skew, which may explain why the data has a vague symmetry. This symmetry is not perfect, however, because the large skew in the $3D$ case has effectively "uncovered" more leading-row turbines. The second mode occurs at $1.5D$ skew, which explains why this location tends to have a local minimum or maximum.

For this skewness study, blockage seems best captured by the box metrics. At $0D$, the farm experiences minimal blockage effects likely due to wind being able to more easily flow between the rows of turbines. As the the skew increases, these pathways become obstructed enhancing the blockage effect. Surprisingly, the blockage effect reduces near $1.5D$. This may be due to the perfect staggering of turbines allowing for easier flow pathways diagonally through the farm. The trend in blockage then reverses until the turbines are once again aligned at $3D$ skew.

3.4 Blockage Outcomes

This series of case studies has provided useful information for how these six blockage metrics might behave during an optimization. The major trend observed between all the case studies was that upstream measurements resulted in velocity slowdown or negative blockage, while overhead measurements resulted in velocity speedup or positive blockage. Additionally, these case studies helped inform our intuition for the types of layouts that produce large blockage effects. Although not a perfect rule of thumb, farms which present a large cross-sectional area relative to the incoming wind, either due to their alignment, spacing, or sheer size are generally more disruptive to the flow and result in larger blockage effects. The idea that blockage is exacerbated by layouts which present as a single, impenetrable obstacle is a useful outcome as we move into the optimization studies.

https://doi.org/10.5194/wes-2022-7
Preprint. Discussion started: 8 February 2022
© Author(s) 2022. CC BY 4.0 License.

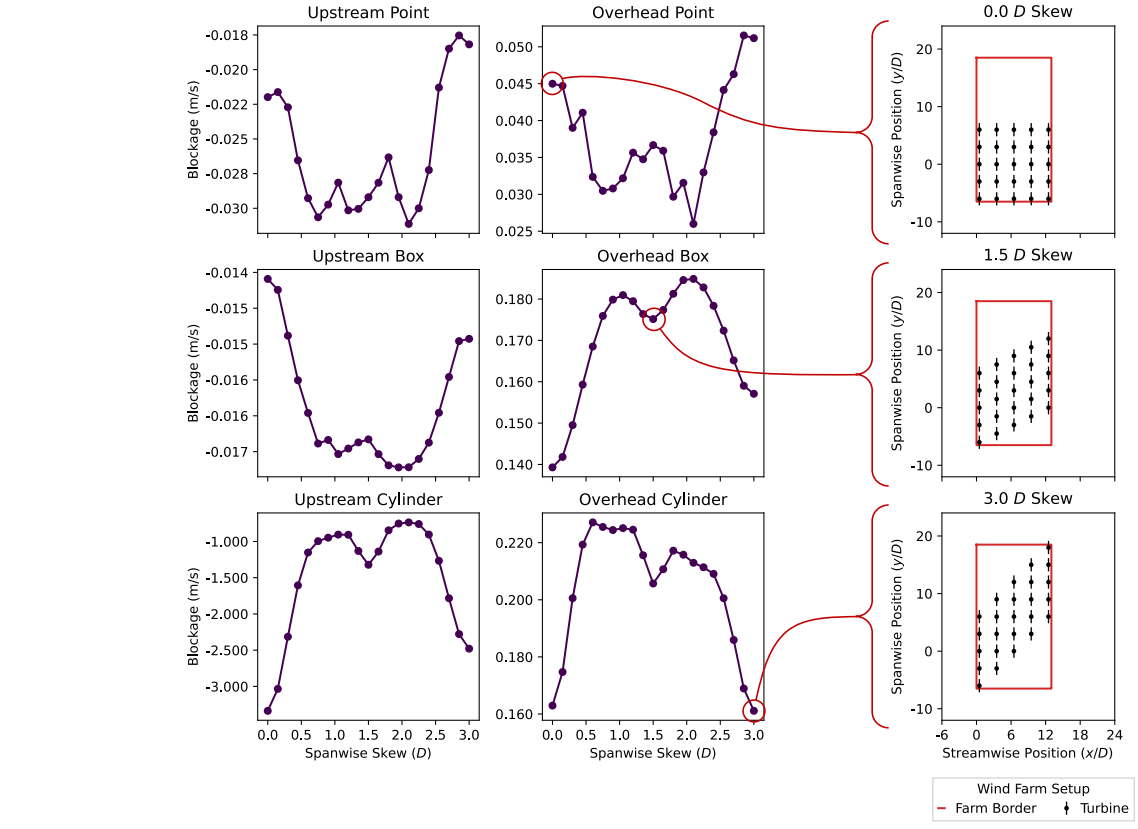

Figure 4. Measured blockage as a function of spanwise skew; Top: the upstream and overhead point measurements, Middle: the upstream and overhead boxes, Bottom: the upstream and overhead cylinders.

4 Optimization Case Studies

Having observed that our blockage metrics can capture the effects of increasing farm size, inter-turbine spacing, and effects due to alignment and skewing, we proceed to design a set of optimization studies. These optimizations are carried out with the understanding that the upstream metrics record a slowdown in the presence of turbines while their overhead counterparts record a speedup. Thus, if the objective function is intended to characterize a minimal disturbance to the surrounding flow, optimization studies using the upstream metrics should be phrased as maximization problems (i.e., drive the negative blockage closer to zero) while studies using the overhead metrics should be phrased as minimization problems (i.e., drive the positive blockage closer to zero). This is a consistent point of view that represents keeping high streamwise velocity closer to the ground where it can generate power rather than redirecting it up and over the farm. These optimizations deviate from the case studies' representation of blockage in that no turbine-free baseline is computed for the calculation $J = J_t - J_b$. Rather, having observed

https://doi.org/10.5194/wes-2022-7
Preprint. Discussion started: 8 February 2022
© Author(s) 2022. CC BY 4.0 License.

eawe european academy of wind energy
Open Access WIND ENERGY SCIENCE DISCUSSIONS

the sign on blockage measurements and formed an understanding of the upstream and overhead variants, we simply maximize or minimize the measured velocity directly.

4.1 Blockage Optimization

We begin by performing a series of layout optimizations using the previous blockage metrics as the sole objective. Although it is probable that these metrics will result in unfavorable layouts from the perspective of power generation, it is useful to understand the patterns and trends that typify a minimal disturbance to the surrounding flow before complicating the layout problem with second-order effects in the form of power considerations. The goal of these optimization is as follows:

$$\begin{aligned} \text{Minimize/Maximize} \quad & f_{\text{blockage}} \\ \text{With respect to} \quad & \text{Turbine Locations} \\ \text{Subject to} \quad & \text{Spacing Constraints} \end{aligned}$$

where the constraint on inter-turbine spacing ensures no two turbines are separated by a distance $< 2D$. The setup for each blockage metric is identical to the case studies from Section 3 with one minor exception. The overhead point metric is now evaluated above the center of the allowable farm bounds. This is because the notion of a leading turbine is difficult to assess when the locations of the turbines change with each optimization step. Evaluating the point directly above the center of the farm attempts to capture what is happening globally rather than restricting the measurement to effects near the western boundary.

For each metric, we ran 20 optimizations each with a random initial layout of 25 turbines each generated with a Latin hypercube sampling procedure. We collected the optimized layouts for all 20 initial conditions and generated a 2D histogram to show where turbines are most likely to be placed. This multistart technique is a powerful tool for revealing global minima in an optimization problem where we suspect individual cases may readily converge to local minima not indicative of global layout trends. These histograms are presented along with boxplots showing the distribution of the initial and optimal objective value for each blockage metric in Figure 5.

The most interesting results come from the overhead point, upstream box, and overhead box metrics. For both box metrics, the optimization tries to place turbines on the north and south extreme of the allowable farm area, which allows wind to flow unimpeded through the farm. In contrast, the overhead point diverts the turbines in the western half of the domain to the north and south edges, but clusters the turbines in the eastern half of the domain in a wedge that extends downstream from the center producing a shape not unlike the starship USS Enterprise. The remaining blockage metrics show little to no overall pattern indicating a significantly multi-modal optimization space.

4.2 Blockage Optimization with Power Constraint

We now turn our attention to a more pragmatic optimization study in which the total power output of the farm is no longer ignored. To determine the trade-off between blockage and power production, we conduct a series of power-constrained blockage optimizations using the ϵ-constraint method Chankong and Haimes (2008) to generate a Pareto front. Specifically, we optimize

https://doi.org/10.5194/wes-2022-7
Preprint. Discussion started: 8 February 2022
© Author(s) 2022. CC BY 4.0 License.

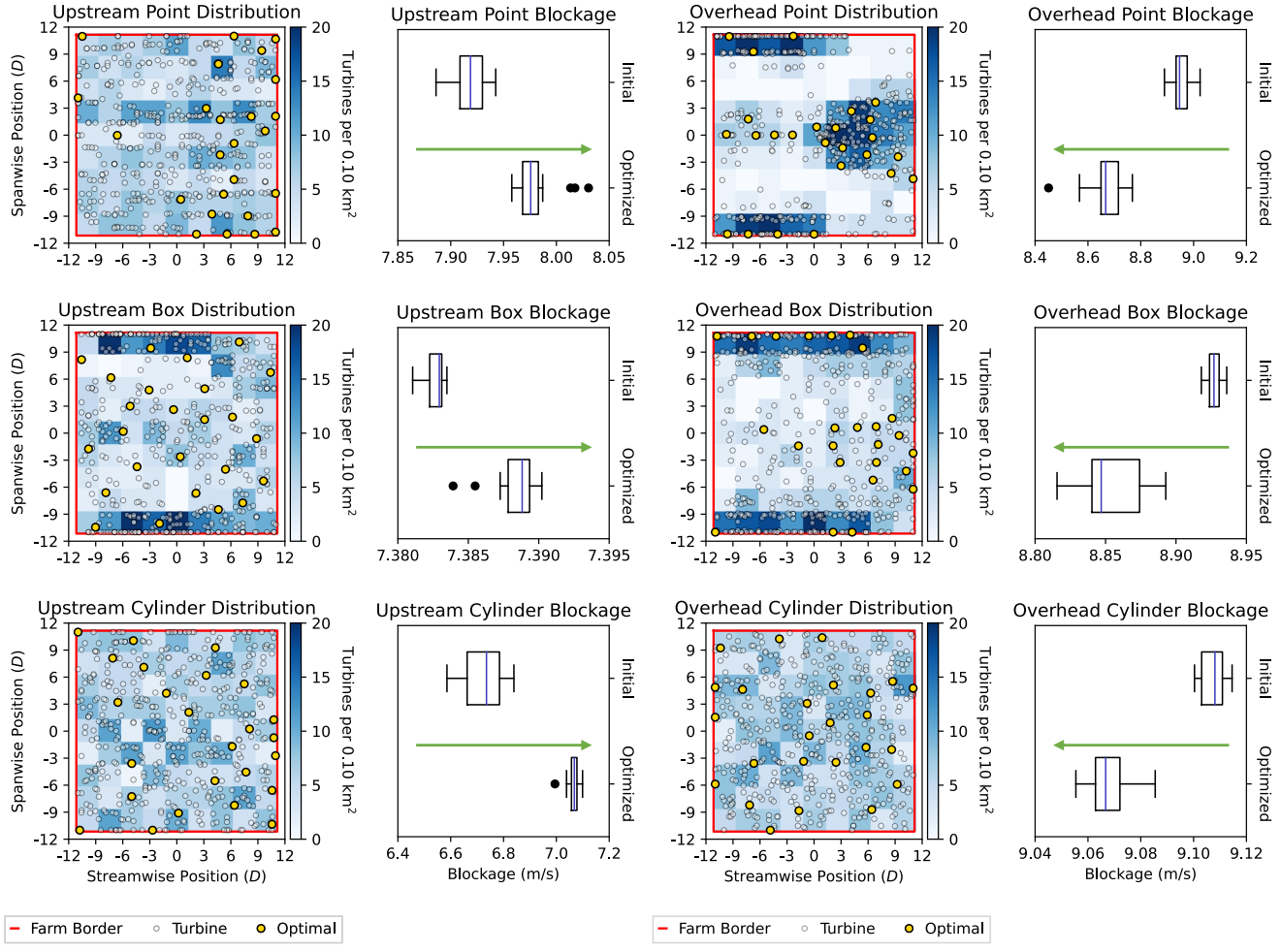

Figure 5. The optimized layout of 25 turbines for all 20 optimizations computed with the respective metric as the objective function; dots represent individual turbines and the histogram highlights the overall trend where the green arrow indicates the direction of improved blockage. Yellow dots mark the single layout which achieved the best blockage outcome. The boxplots for both the the initial layout configurations and the optimal configurations is provided to show the improvement.

https://doi.org/10.5194/wes-2022-7
Preprint. Discussion started: 8 February 2022
© Author(s) 2022. CC BY 4.0 License.

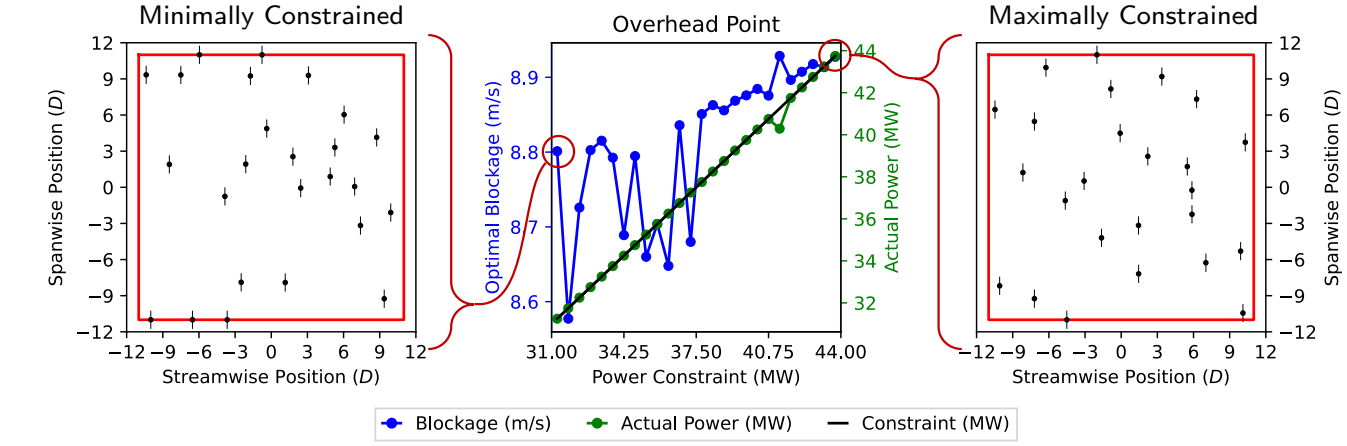

Figure 6. The optimized blockage, measured power, and layouts associated with carrying out layout optimizations while satisfying a variable minimum power threshold in the range $[31.25, 43.75]$ MW.

the blockage metric while requiring a minimum power production from the farm and repeat this process for a sweep of minimum power requirements. A Pareto front could also be obtained by performing a weighted bi-objective optimization, but by using the ϵ-constraint method we more accurately capture the true Pareto front by circumventing spurious trends caused by the convexity of sweeping a weighted bi-objective space.

We determine the minimum bounds of the power constraint by using the lowest power output cases produced by the previous blockage optimization studies, whereas the maximum bounds come from yet another series of multistart optimizations in which total farm power was the sole objective. This results in a set of power constraints ranging from 31.25 MW to 43.75 MW. The initial condition for each optimization in this sweep is the randomized layout from the study presented in Section 4.1 that produced the highest power. The overhead point metric was chosen for this power-constrained optimization due to the clear trend emerging in Figure 5 and the desire to achieve easily recognizable layout modes associated with the extreme cases where the minimum power requirement takes on either the minimum or maximum value. As before, we attempt to minimize the overhead measurement with the understanding that this represents reduced blockage. The blockage, measured power, and layout resulting from these power-constrained optimizations is shown as a function of the power constraint in Figure 6.

As seen in Figure 6, the power constraint has a significant effect on the resulting layout. At the minimum required power of 31.25 MW, the optimizer has a high degree of freedom to explore blockage-optimal turbine arrangements and returns a layout that very closely matches the histogram shown in Figure 5. At the other extreme, satisfying a minimum power constraint of 43.75 MW yields a turbine arrangement that has very little resemblance to the blockage-optimized layout; instead, the turbines have become separated and staggered in the spanwise direction such that effects due to waking are diminished. The behavior between these two endpoints is depicted by the line plots, in which a superior reduction in the overhead blockage tends to cede importance to power output as the power constraint takes on increasingly large values. It is interesting to note that in all cases but one, the actual power produced by the optimized layout exactly matches the power constraint as expected. In the single

https://doi.org/10.5194/wes-2022-7
Preprint. Discussion started: 8 February 2022
© Author(s) 2022. CC BY 4.0 License.

outlier case, the measured blockage attains its highest value, which may be explained by an unusually high-blockage turbine configuration creating a numerically difficult solution from which the optimizer cannot recover. It is possible that increasing the penalty for violating the minimum power constraint could rectify the behavior in this case.

Finally, it should be noted that although stronger blockage effects are clearly associated with higher power output layouts, the trend in our results is not monotonically increasing. We attribute this to the appreciable probability of a single optimization converging to a local minima which appears to contradict the more global trend. Repurposing the multistart approach from Section 4 may help illuminate this blockage-power trade off more clearly.

5 Concluding Remarks

The investigatory nature of Section 3 leads us to respond to the question of which metric best represents blockage. As mentioned in the introduction, the two primary motivations for investigating blockage are determining the effect a farm will have on far-field flow and explaining the discrepancy between predicted power production and actual power production. Studying the latter is hindered by the need to collate experimental power data, and so for now, we focus on the effects on far-field flow in the context of criteria (i)–(iii) introduced in Section 1.

With these three considerations in mind, we evaluate the 3 metrics and 2 orientation variants presented. The cylinder metrics are difficult to dissect. Though in most of the case studies, they performed somewhat intuitively, the fact that the optimizations resulted in no discernible pattern implies that they lead to severely multi-modal optimizations. This makes them difficult to use as an objective function unless coupled with more constraints. Additionally, the fact that the upstream variant routinely incorporates wake effects somewhat diminishes their value as a measure of blockage using the definitions given previously.

We then turn our attention to the points and boxes. In all case studies, the point metrics proved to be difficult to reliably deploy, where small changes in the probe location or overall mesh could result in significant changes in behavior. This sensitivity likely stems from its limited scope in terms of capturing farm-wide effects. However, the point metrics are perhaps the best proxy for experimental data obtainable from MET towers, and for this reason alone may prove useful for future validation studies concerning predicted and actual power output for a given site.

In contrast to the limited-field view of the points, the box metrics capture a window that can be expanded to cover the entire area of the farm and are not subject to waking effects in the farm interior if positioned carefully. As such, they appropriately address the first of our criteria. Additionally, this large area of integration makes them more robust to mesh resolution and placement. Computationally, they are relatively easy to implement and behave well on distributed hardware. By these evaluation criteria, and taking into account the optimization results from Figure 5, the upstream box shows perhaps the most potential as a useful blockage metric.

Further analyzing the optimization results presented in Section 4.1 helps answer this question more fully as they reveal several clear trends that exemplify the layout of minimal-blockage farms. When quantifying blockage with a single point source, the overhead metric leads to more pronounced outcomes than the upstream point, but the reason for this significantly different behavior is not clear. In blockage test cases 3.1-3.3, the upstream point metric roughly follows the behavior of the

https://doi.org/10.5194/wes-2022-7
Preprint. Discussion started: 8 February 2022
© Author(s) 2022. CC BY 4.0 License.

upstream box both in both a qualitative and quantitative sense. But where the upstream box optimizations favor placing turbines in streamwise rows, such a global trend does not emerge for the upstream point. A more in-depth analysis of the fluid behavior around the upstream measurement point may shed light on how to improve these optimizations.

Returning to the box measurements, both the upstream and overhead variants produce the aforementioned streamwise alignment. It is reassuring to see this trend recovered in both cases, as the same farm design that maximizes streamwise velocity through a large, projected area upstream of the farm seems to intuitively satisfy that it must also result in a decrease in the streamwise velocity through a large area passing up and over the farm. The ability to reliably capture these global trends leads us to reiterate the suggestion that the box metric best captures the blockage effect.

In the course of this investigation we considered the possibility of combining one or more measurement techniques to characterize blockage even more fully. For example, a weighted metric that combines the notion of maximizing velocity through an upstream box while also minimizing the flow as measured by one or more strategically-located overhead points. Such a hybrid approach was beyond the scope of the more systematic testing we present here but is an interesting target for future work. Evaluating these solutions in a study that focuses on predicted versus actual power output for new-farm construction—where the latter may be observed to under perform due to unaccounted for blockage effects—is of particular interest as we continue to study the trade-off between power and blockage.

Code and data availability. The data that support the findings of this study are available from the corresponding author upon reasonable request. The open-source software used to produce the results and analyses presented in this manuscript are available through the `WindSE` GitHub repository: https://github.com/NREL/WindSE.

Author contributions. Ethan Young, Jeffery Allen, and John Jasa developed and tested the blockage metrics, defined and implemented the optimization problems, and carried out the final production runs on the HPC. Garrett Barter helped define the optimization problems, refined the presentation of results, and helped frame the importance of the blockage phenomenon around power generation. Ryan King provided yet another perspective on the importance of blockage for new plant construction and helped modify and refine the CFD simulations and blockage definitions. Ethan Young prepared the manuscript with contributions from all co-authors.

Competing interests. The authors declare that they have no conflict of interest.

Acknowledgements. This work was authored by the National Renewable Energy Laboratory, operated by Alliance for Sustainable Energy, LLC, for the U.S. Department of Energy (DOE) under Contract No. DE-AC36-08GO28308. Funding provided by the U.S. Department of Energy's Wind Energy Technologies Office. The views expressed in the article do not necessarily represent the views of the DOE or the U.S. Government. The U.S. Government retains and the publisher, by accepting the article for publication, acknowledges that the U.S.

https://doi.org/10.5194/wes-2022-7
Preprint. Discussion started: 8 February 2022
© Author(s) 2022. CC BY 4.0 License.

eawe european academy of wind energy
Open Access WIND ENERGY SCIENCE DISCUSSIONS

Government retains a nonexclusive, paid-up, irrevocable, worldwide license to publish or reproduce the published form of this work, or allow others to do so, for U.S. Government purposes.

This research was performed using computational resources sponsored by the Department of Energy's Office of Energy Efficiency and Renewable Energy and located at the National Renewable Energy Laboratory

We would like to acknowledge Christopher Bay for participating in fruitful discussions regarding the role of blockage and how to best quantify its effect.

https://doi.org/10.5194/wes-2022-7
Preprint. Discussion started: 8 February 2022
© Author(s) 2022. CC BY 4.0 License.

eawe european academy of wind energy
Open Access WIND ENERGY SCIENCE DISCUSSIONS

References

Allen, J., King, R., and Barter, G.: Wind Farm Simulation and Layout Optimization in Complex Terrain, Journal of Physics: Conference Series, 1452, 012 066, https://doi.org/10.1088/1742-6596/1452/1/012066, 2020.

Allen, J., Young, E., Bortolotti, P., King, R., and Barter, G.: Blade Planform Design Optimization to Enhance Turbine Wake Control, Wind Energy, In Final Review.

Bleeg, J., Purcell, M., Ruisi, R., and Traiger, E.: Wind Farm Blockage and the Consequences of Neglecting Its Impact on Energy Production, Energies, 11, https://doi.org/10.3390/en11061609, 2018.

Bortolotti, P., Tarres, H. C., Dykes, K., Merz, K., Sethuraman, L., Verelst, D., and Zahle, F.: IEA Wind Task 37 on Systems Engineering in Wind Energy – WP2.1 Reference Wind Turbines, National Renewable Energy Lab Report NREL/TP-73492, 2019.

Branlard, E., Quon, E., Forsting, A. R. M., King, J., and Moriarty, P.: Wind farm blockage effects: comparison of different engineering models, in: Journal of Physics: Conference Series, vol. 1618, p. 062036, IOP Publishing, 2020.

Chankong, V. and Haimes, Y. Y.: Multiobjective decision making: theory and methodology, Courier Dover Publications, 2008.

Funke, S. W. and Farrell, P. E.: A framework for automated PDE-constrained optimisation, CoRR, abs/1302.3894, 2013.

Gill, P. E., Murray, W., and Saunders, M. A.: SNOPT: An SQP algorithm for large-scale constrained optimization, SIAM Journal of Optimization, 12, 979–1006, https://doi.org/10.1137/S1052623499350013, 2002.

Logg, A., Mardal, K.-A., Wells, G. N., et al.: Automated Solution of Differential Equations by the Finite Element Method, Springer, https://doi.org/10.1007/978-3-642-23099-8, 2012.

Lyu, Z., Xu, Z., and Martins, J. R. R. A.: Benchmarking Optimization Algorithms for Wing Aerodynamic Design Optimization, in: Proceedings of the 8th International Conference on Computational Fluid Dynamics, Chengdu, Sichuan, China, iCCFD8-2014-0203, 2014.

McTavish, S., Feszty, D., and Nitzsche, F.: An experimental and computational assessment of blockage effects on wind turbine wake development, Wind Energy, 17, 1515–1529, https://doi.org/https://doi.org/10.1002/we.1648, 2014.

McTavish, S., Rodrigue, S., Feszty, D., and Nitzsche, F.: An investigation of in-field blockage effects in closely spaced lateral wind farm configurations, Wind Energy, 18, 1989–2011, https://doi.org/https://doi.org/10.1002/we.1806, 2015.

NREL: FLORIS. Version 2.4, https://github.com/NREL/floris, 2021a.

NREL: WindSE: Wind Systems Engineering Version 2021.08.01, https://github.com/NREL/WindSE, 2021b.

Nygaard, N. G., Steen, S. T., Poulsen, L., and Pedersen, J. G.: Modelling cluster wakes and wind farm blockage, Journal of Physics: Conference Series, 1618, 062 072, https://doi.org/10.1088/1742-6596/1618/6/062072, 2020.

Quon, E., Sandhu, R., Thedin, R., Doubrawa, P., Draxl, C., Lawson, M., Tripp, C., Williams, L., Farmer, C., and Katzner, T.: Golden Eagle Behavioral Modeling Enabled by High-Fidelity Atmospheric Models, Tech. rep., National Renewable Energy Lab, Golden, CO (United States), 2021.

Wu, N., Kenway, G., Mader, C. A., Jasa, J., and Martins, J. R. R. A.: pyOptSparse: A Python framework for large-scale constrained nonlinear optimization of sparse systems, Journal of Open Source Software, 5, 2564, https://doi.org/10.21105/joss.02564, 2020.